Supporting Information

Conductive and Antibacterial Dual Network Hydrogel for Soft Bioelectronics

Huiqi Sun, Sai Wang, Fan Yang, Mingyi Tan, Ling Bai, Peipei Wang, Yingying Feng, Wenbo Liu, Rongguo Wang, and Xiaodong He*

H. Sun, Prof. F. Yang, M. Tan, L. Bai, P. Wang, Y. Feng, Prof. W. Liu, Prof. R. Wang, Prof. X. He
National Key Laboratory of Science and Technology on Advanced Composites in Special Environments, Harbin Institute of Technology
Harbin 150000, P. R. China
E-mail: wrg@hit.edu.cn (Prof. R. Wang)

Dr. S. Wang
School of Mechatronic Engineering, Shenzhen Polytechnic
Shenzhen 518055, P. R. China

This file includes

Figures S1 to S25

Tables S1 to S5

References

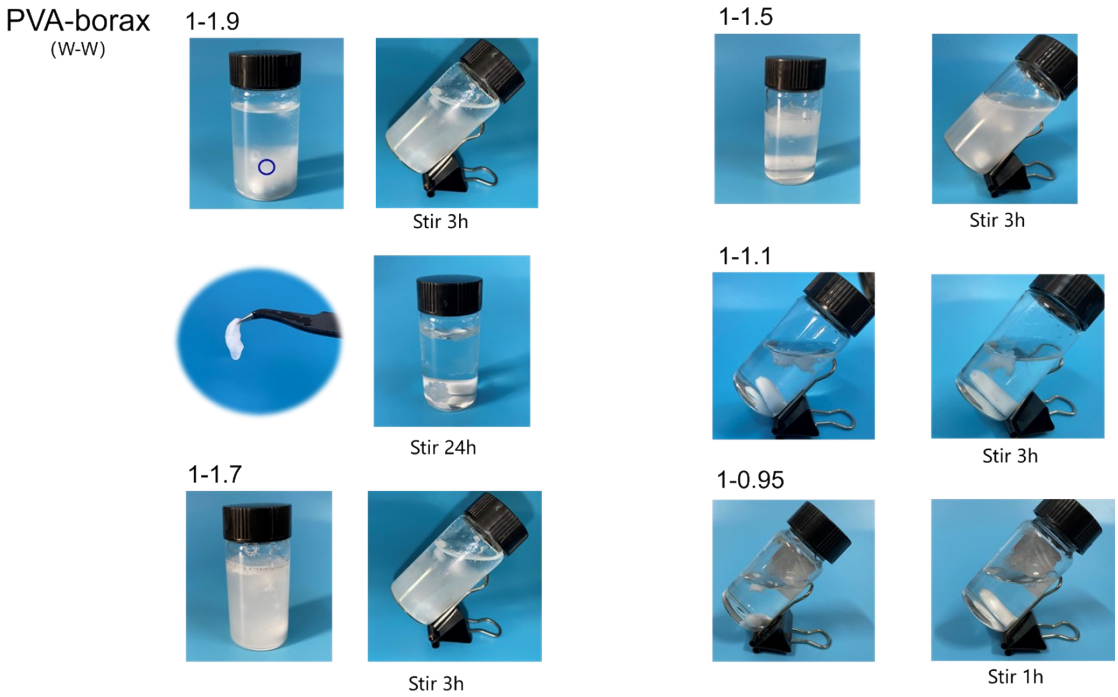

Figure S1. The physical appearance of PVA-borax with different weight ratios in the hydrogel precursor solution.

Note 1

It is well known that borax ($Na_2B_4O_7 \cdot 10H_2O$) is a good buffer. When hydrolyzed in water, borax easily dissociated into boric acid and borate ions. Borax reacts with the hydroxyl groups of PVA chains, forming interchain dynamic diol−borax complexation as the crosslink sites in the network, which leads to gelation quickly. According to Leibler et al.,[1] the structure of the PVA–borate complex in an aqueous solution depends on the following factors:

1. The intramolecular/intermolecular crosslinking reactions of PVA and borate
2. The charge repulsion among the complex units
3. The electrostatic screen effect on the negative-charge complex unit by free ions

Combined with the above factors, we have made some attempts to make the gelation process more controllable at room temperature, including adding acrylic and glycerin to the PVA solution. On the one hand, glycerin, as a polyhydric alcohol, can react and chelate with borax preferentially;[2] on the other hand, acrylic can create a faintly acidic environment (PH≈5). Thus, the two aspects decrease the amount of borax instant crosslinking with PVA, increasing the stable borax existence content in the PVA solution at room temperature (PVA-borax 1-0.95), Although it was higher than the other reports, [2,3] the pure borax accounted for only 0.71 wt% of the total solution (PVA-borax 1-0.95).

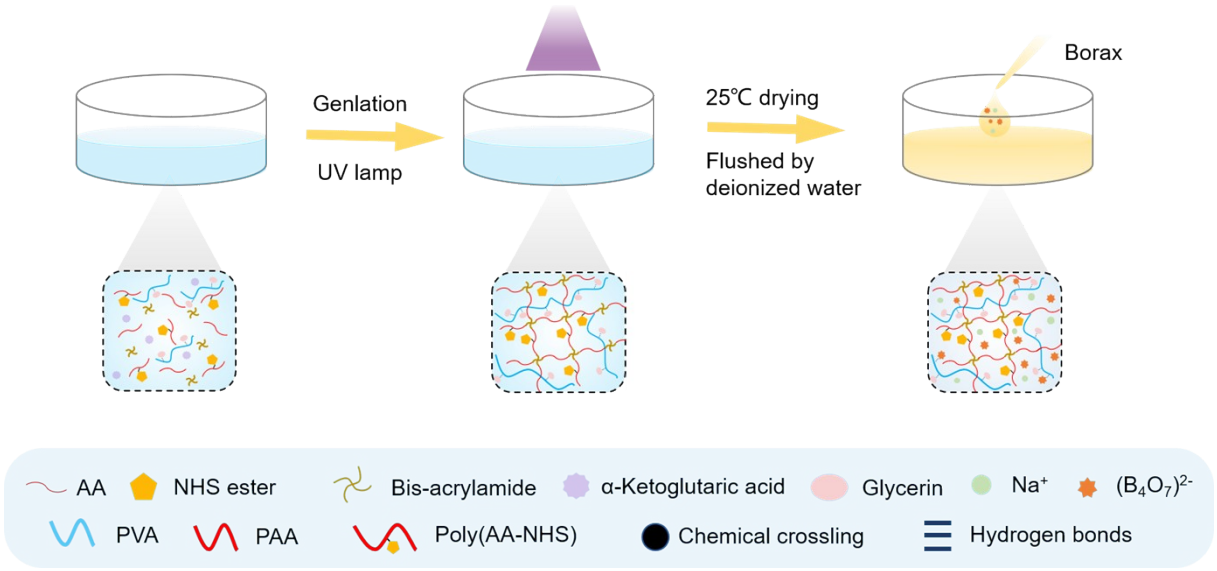

Figure S2. Preparation of the conductive hydrogel.

Note 2

Briefly, acrylic acid (AA), acrylic acid N-hydroxysuccinimide ester (AA-NHS), PVA, and glycerin were successively added to the water with continuous stirring until a transparent homogeneous mixture was obtained. Afterward, the hydrogel precursor solution was cured with UV irradiation from the hydrogel network. Upon 25°C air drying for 6 hours, the hydrogel was rehydration in the 0.1M borax solution, not only introducing borax into the network by the hydrogel intrinsic swelling behavior but also removing monomers and other small molecule residues. Finally, a transparent, soft, adhesive with multifunction conductive hydrogel was obtained.

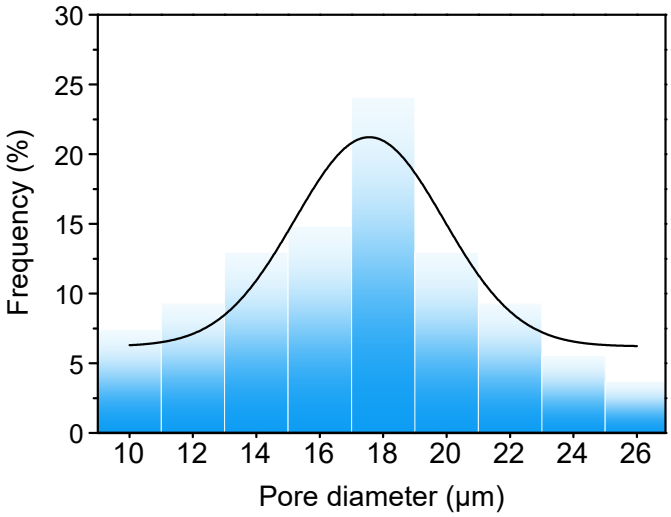

Figure S3. Pore size distribution for conductive hydrogel. The pore sizes of hydrogel were obtained from the SEM images by randomly selecting 50 pores in a field of view.

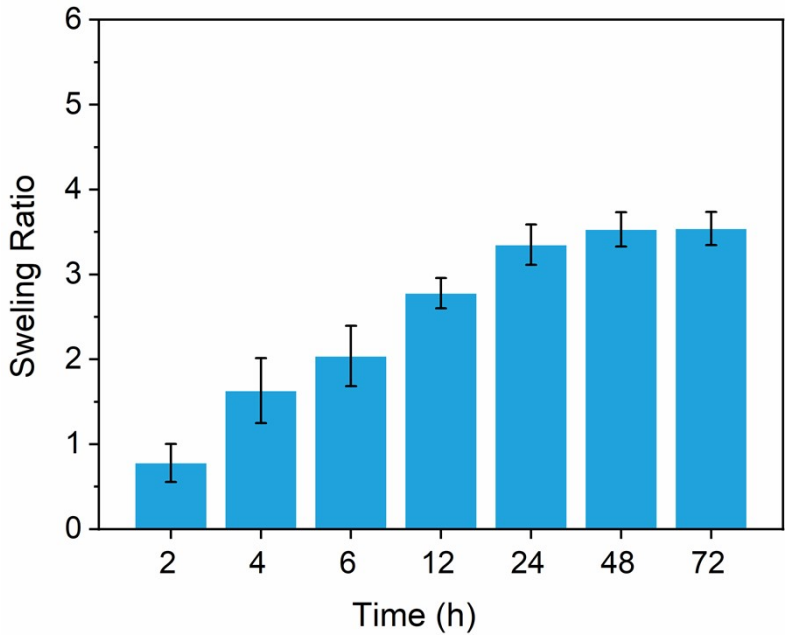

Figure S4. Swelling of hydrogels incubation in PBS at 37 ℃.

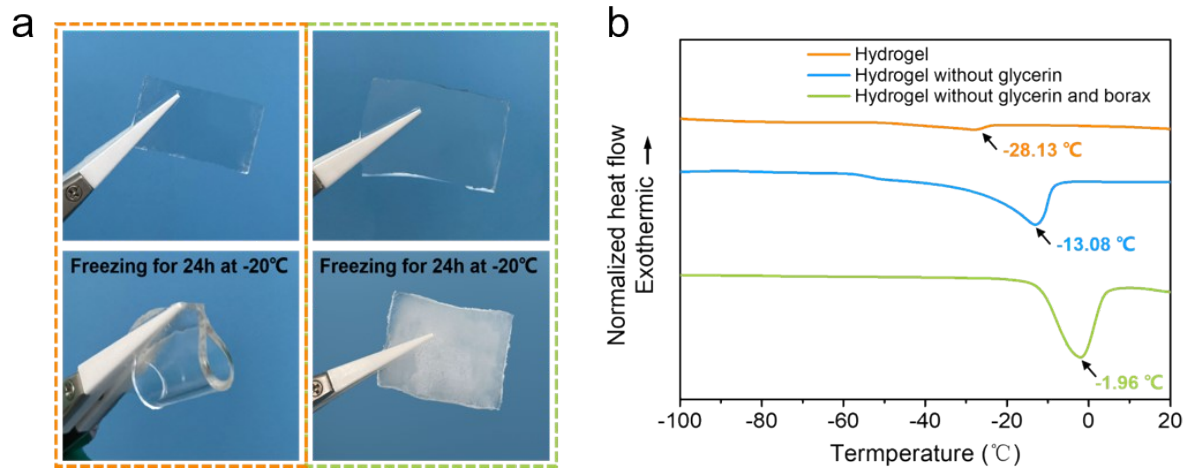

Figure S5. a) Digital photos of hydrogel and hydrogel without glycerin and borax before and after freezing at -20℃ for 24h.b)DSC curves of different components of hydrogels.

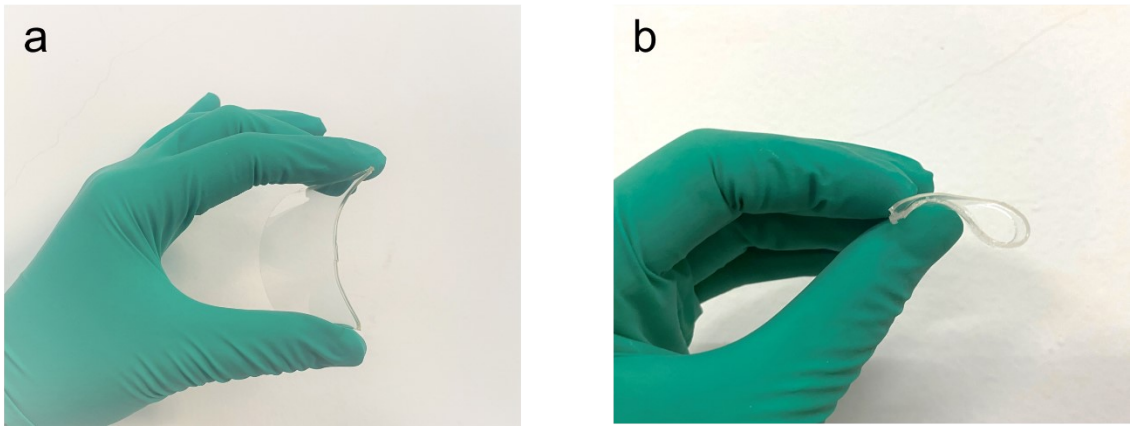

Figure S6. Digital photos of pure hydrogel (a) and hydrogel-borax/glycerin (b) after storage at the normal environment (25℃, 60% RH) room temperature for 14 days.

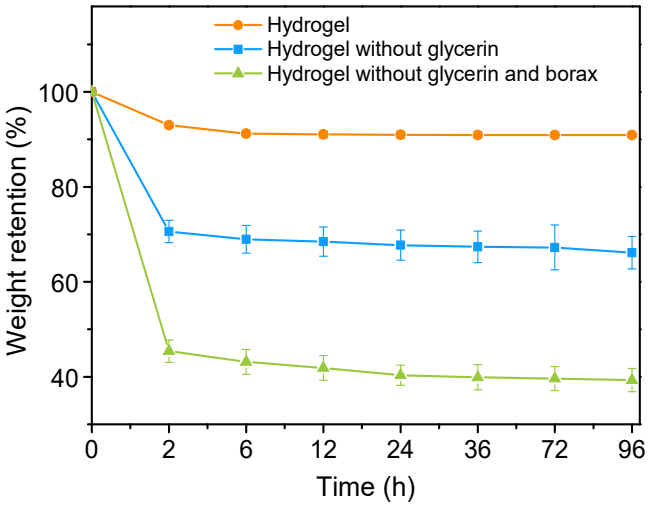

Figure S7. Weight retention of the different components of hydrogels after 96h at 25℃ and 10% relative humidity.

Note 3

Differential scanning calorimetry (DSC) tests of three prepared samples were conducted to further systematically investigate the anti-freezing properties (Fig. S5). Compared with the crystallization peak of pure hydrogel, the endothermic peak of hydrogel-borax decreased from -1.96℃ to -13.08℃. This phenomenon was because inorganic salt ions (borax) were introduced into the hydrogel network to decrease the freezing point of free water in the hydrogel network, which relies on the colligative property of ionic compounds to depress the freezing point of the aqueous phase.[4] Furthermore, with the introduction of glycerin, the peak positions shifted rapidly to the negative direction, and hydrogel-borax/glycerin exhibited a lower endothermic peak at -28.13℃. The results indicated glycerin and borax have a synergistic effect on enhancing the anti-freezing ability of hydrogels. Glycerin can form strong hydrogen bonds with H2O molecules, thus disrupting the formation of ice crystal lattices at subzero temperatures. In order to visually demonstrate the frost resistance of hydrogels, without borax and glycerin hydrogel and hydrogel-borax/glycerin were stored at -20 ℃ for 24 h to observe their morphology changes. As shown in Fig. S5, it was clearly observed that pure hydrogel was frozen completely and changed from transparent to opaque, losing its elasticity. However, as proposed hydrogel kept the origin transparent and could bear arbitrary deformations such as bending and multiple distortions, exhibiting excellent anti-freezing behavior. In addition, weighting experiments confirm the water retention capacity of the hydrogel-borax/glycerin (Fig. S6 and S7). When the samples were exposed to a drying oven (at 25℃ and 10% relative humidity), the mass loss of hydrogel-borax/glycerin was less than 10% after 96h, whereas the pure hydrogel loss of almost 60%. After storing at room temperature for 14 days, the pure

hydrogel loses flexibility and becomes stiff, but the hydrogel-borax/glycerin still can be folded, firmed its good environmental tolerance.

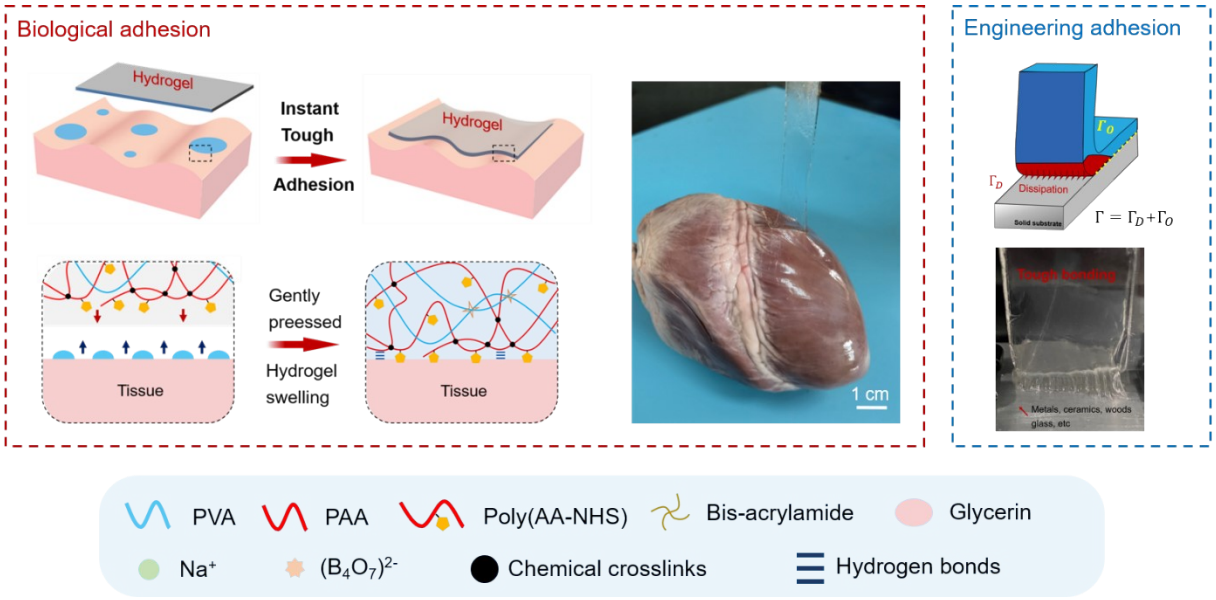

Figure S8. Schematic diagram of hydrogel adhesion to different kinds of materials. When the hydrogel contacted wet tissue, the hydration barrier was adsorption and removed by numerous hydrophilic groups. With increasing adhered time, the covalent crosslinks were formed by the amide bond between the NHS and amine moieties, which provide stable, robust adhesion. It can be clearly seen that the hydrogel-solid adhesive interface exist a large mechanical dissipation during the peeling process, which further contributes to the adhesive strength.

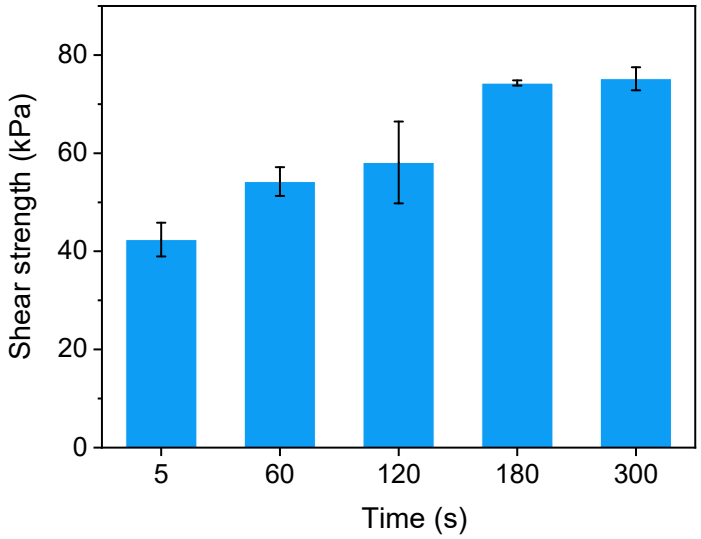

Figure S9. Effect of the contacting time on the adhesion performance. Shear strength versus contacting time for wet porcine skins adhered with our hydrogels. Data are presented as mean ± S.D., $n = 3$.

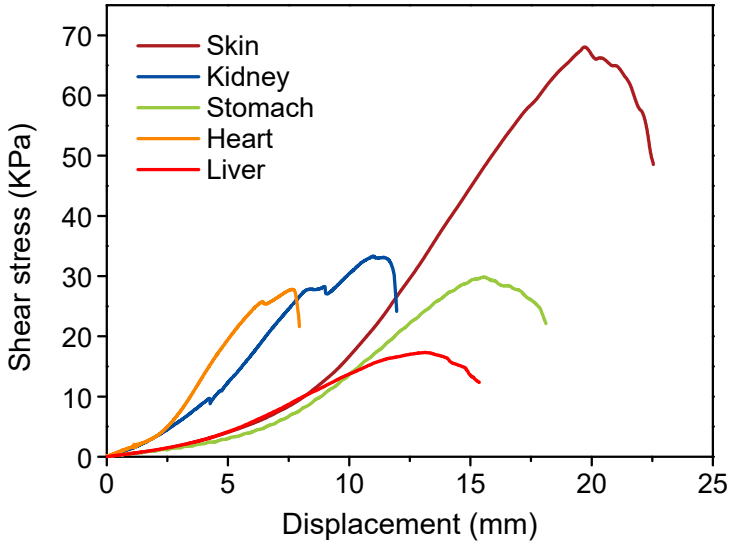

Figure S10. The representative lap shear test curves the shear strength between different organs (skin, kidney, stomach, heart, liver) and hydrogel.

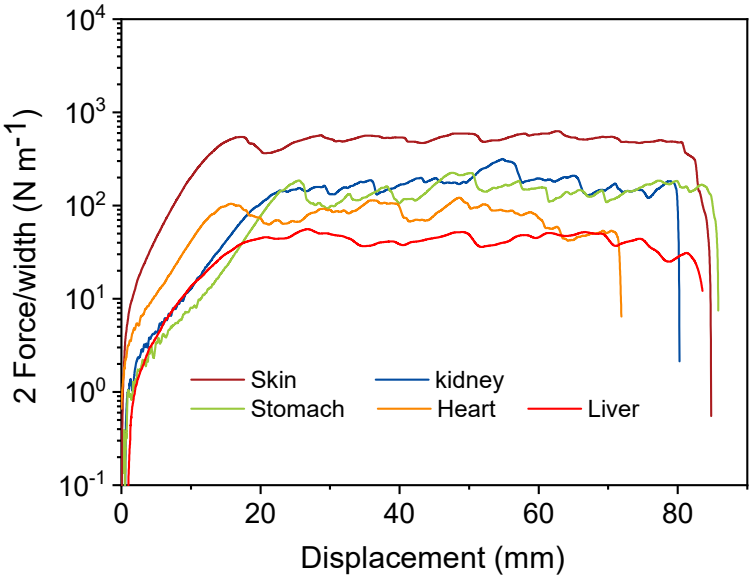

Figure S11. The representative 180° peeling test curves the interfacial toughness between different organs (skin, kidney, stomach, heart, liver) and hydrogel.

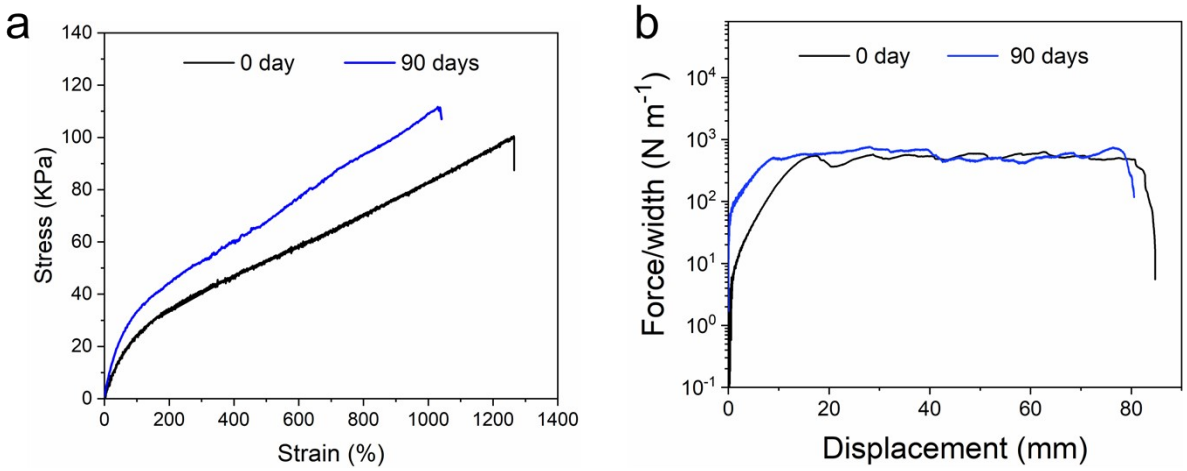

Figure S12. a) The mechanical test of the hydrogel before and after 90 days of storage at 25℃; b) The 180° peeling test curves the interfacial toughness between the porcine skin and hydrogels before and after 90 days of storage at 25℃.

As seen in Fig. S12, the adhesion stability also be well demonstrated. The adhesive properties of the hydrogels were slightly increased after 90 days of storage, which was due to the improved mechanical properties caused by the slight dehydration of hydrogel

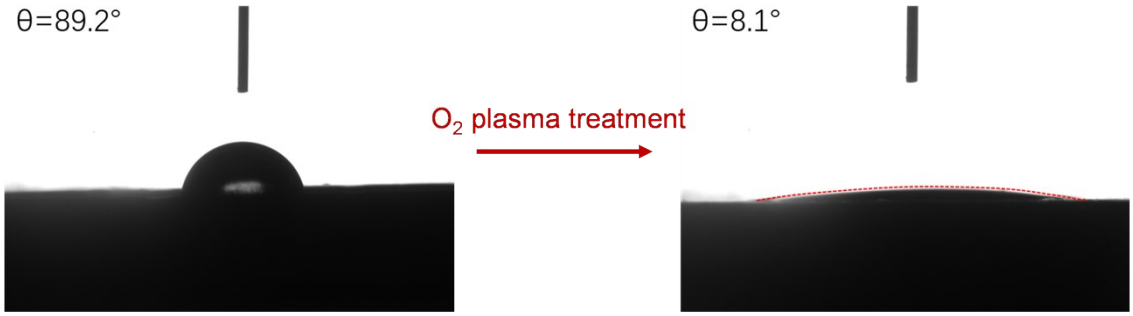

Figure S13. Oxygen plasma treatment of the aluminum sheet, the water contact angle changed from 89.2° to 8.1°.

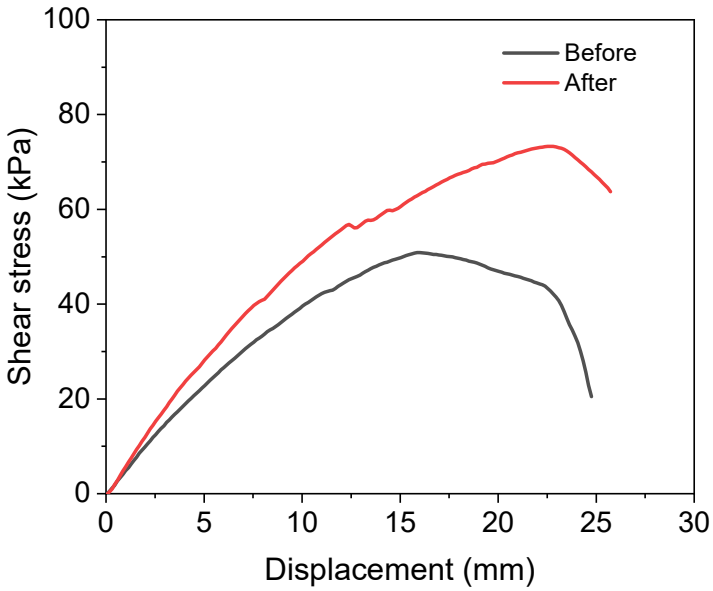

Figure S14. The shear strength before and after the oxygen plasma treatment of the aluminum sheets.

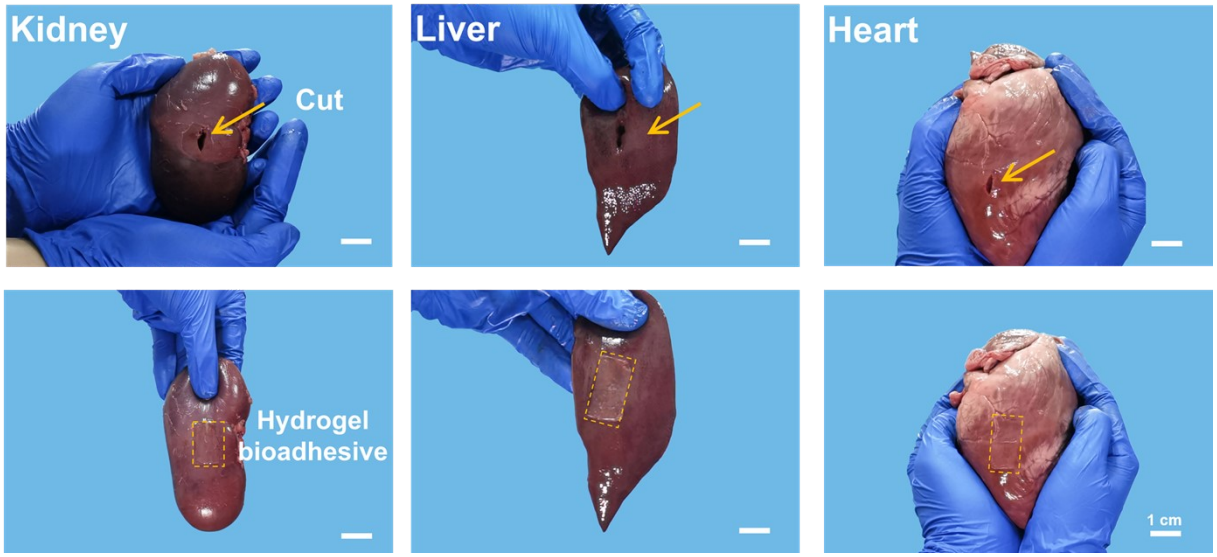

Figure S15. Image of ex vivo tissue sealant for the use of hydrogel.

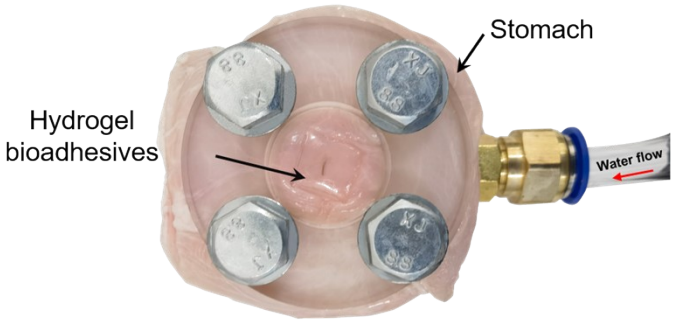

Figure S16. Photograph of home-made setup for the quantification of burst pressure.

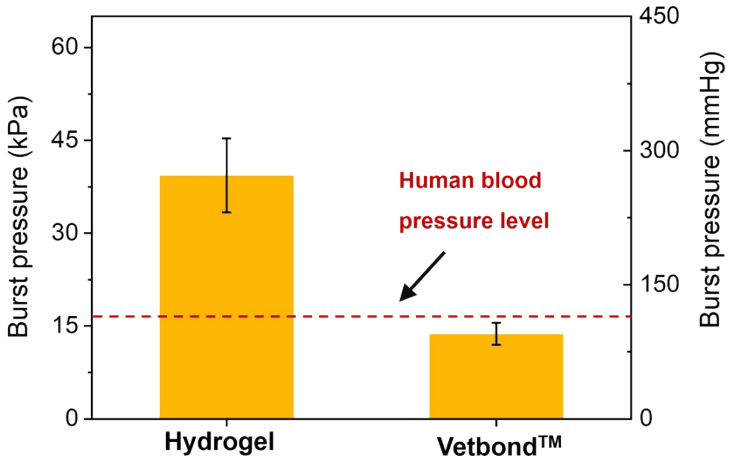

Figure S17. The burst pressure comparison of hydrogel and commercial sealant produc

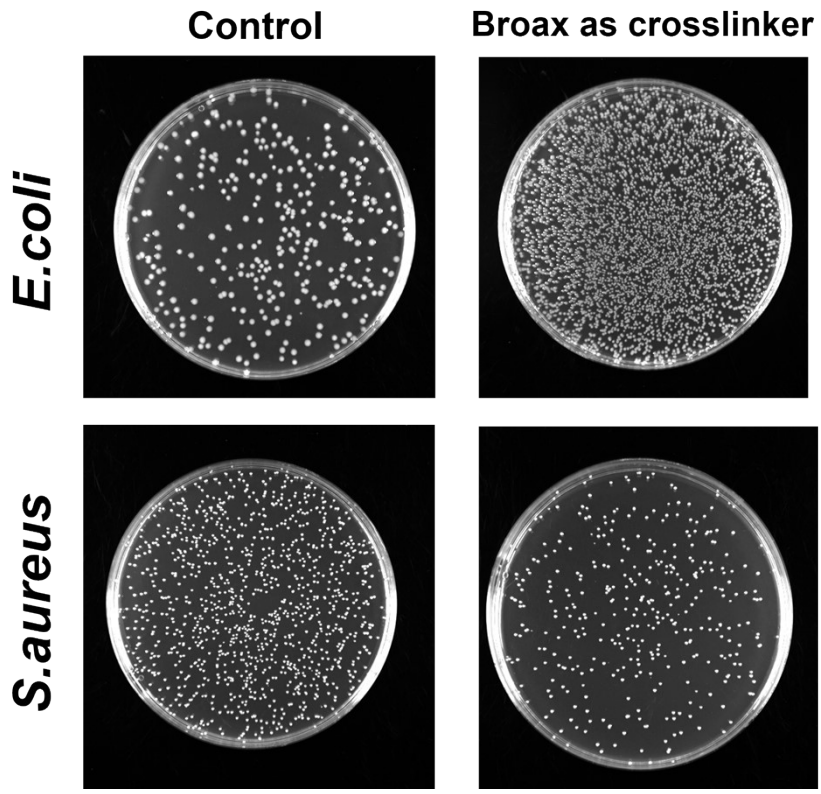

Figure S18. In vitro antibacterial activities borax as crosslinker hydrogel against *S.aureus* and *E.coli.*

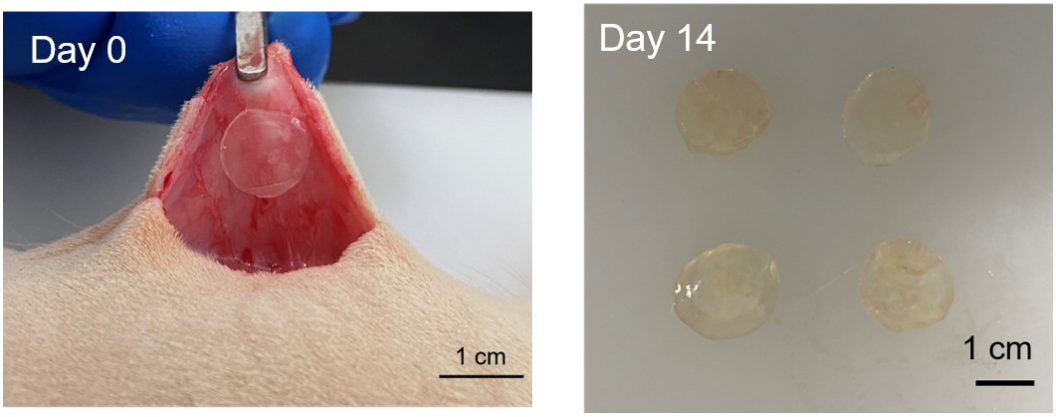

Figure S19. The swelling behaviors of hydrogel in the rat subcutaneously for two weeks. The hydrogel exhibits a slight swelling in an in vivo environment due to the osmotic pressure

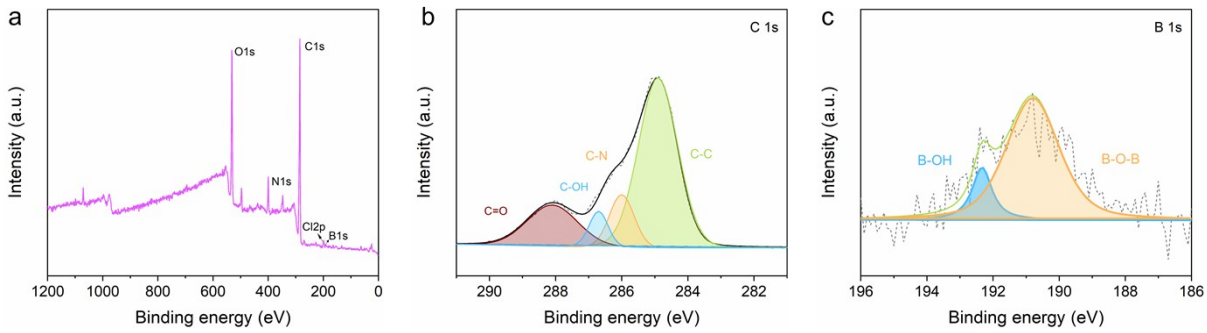

Figure S20. a) XPS general scan spectra, b) C1s spectra, and c) B1s spectra of the hydrogel after subcutaneous implantation for 14 days.

As depicted in Fig. S20 and Table S3, the results solidify the presence of borax within the hydrogel even throughout the implantation period and ensuing elution process.

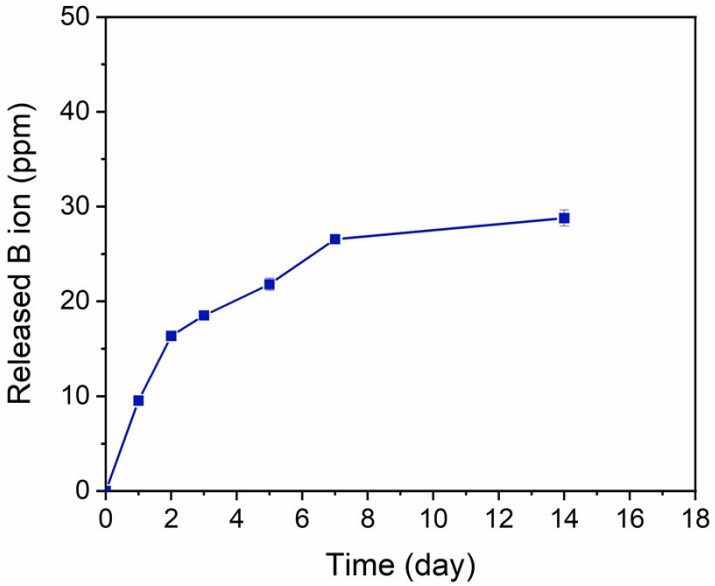

Figure S21. B ion-release profile of hydrogel, as measured using ICP-MS.

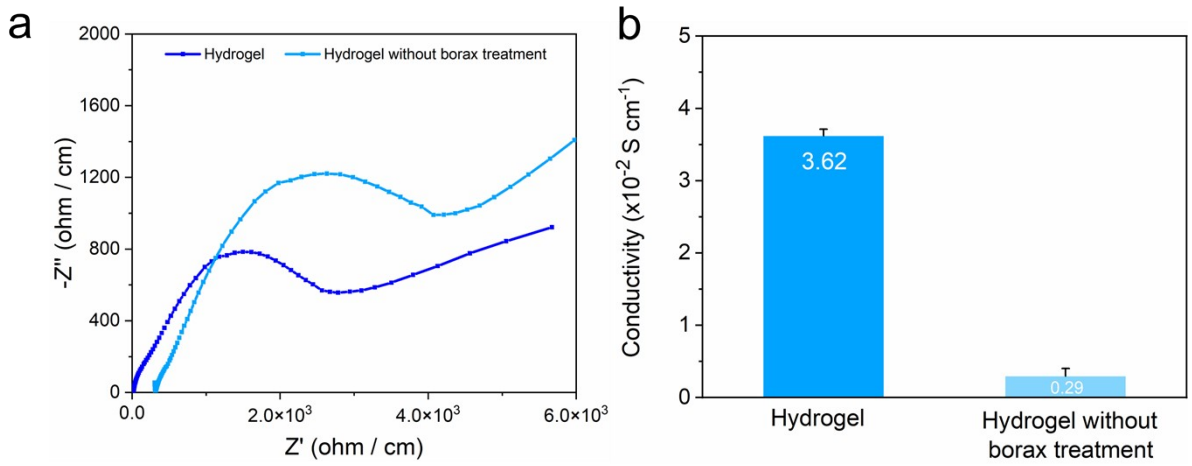

Figure S22. a) EIS Nyquist plot and b) The conductivity comparison of the hydrogel before and after borax treatment.

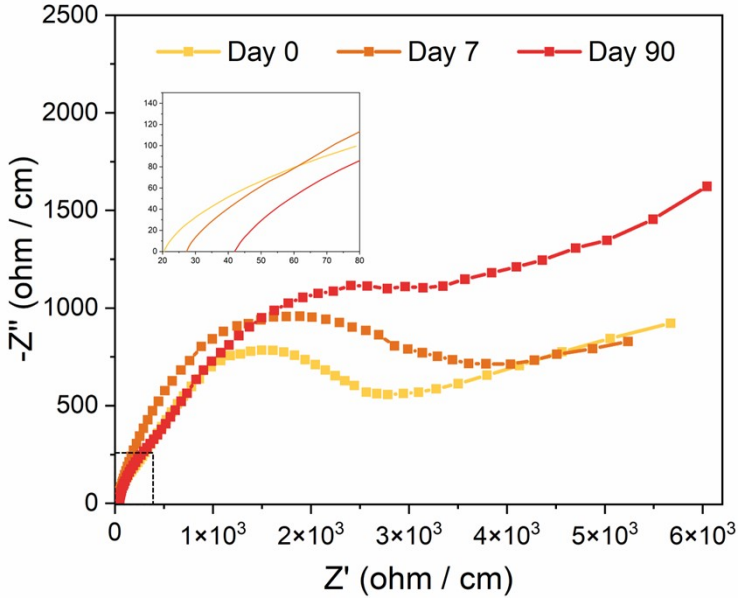

Figure S23. EIS Nyquist plot of the hydrogel stored at room temperature over three months.

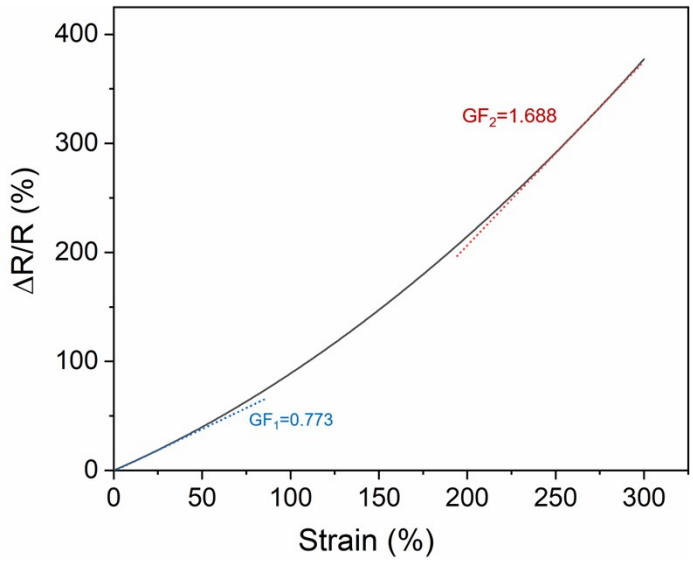

Figure S24. The gauge factor (GF) with the increase of tensile strain. GF_1 and GF_2 are the calculated sensitivities

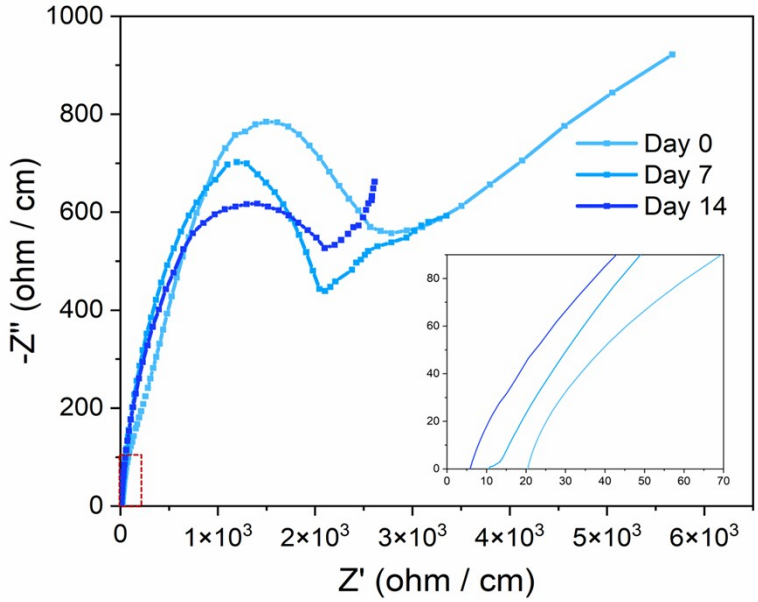

Figure S25. EIS Nyquist plot of the hydrogel implanted in the rat's subcutaneous tissue over two weeks.

Table S1. Comparison of elastic/storage modulus of organs.

Organs	Modulus	Reference
Brain	G'=0.9~1.6 kPa	5
Heart	G'=30 kPa	5
Medulla	G'=3.8 kPa	6
Nerve	G'≈21-400 kPa	7
Cervix tissue	G'=4.7~6.3 kPa	8
Liver & Kidney	E~190 kPa	9-12
Artery & Vein	E~125 kPa	13-16
Muscle	E~7 kPa	10,17
Our hydrogel	**G'=12 kPa**	**This work**

Table S2. The atomic percentage of elements (at%) obtained from XPS spectra after borax treatment of hydrogel.

Element [at%]				
C	O	N	B	Na
72.79	23.3	0.58	3	0.33

Table S3. The atomic percentage of elements (at%) obtained from XPS spectra of the hydrogel after implanted in the rat's subcutaneous tissue over two weeks.

Element [at%]					
C	O	N	B	Na	Cl
68.91	19.81	7.56	2.24	0.84	0.64

Table S4. Comparison of different bioadhesives and their wet tissue adhesion performance.

Materials & Forms	Adhesion speed	Wet adhesion properties	Adhesion condition	Antibacterial properties	Wound Healing/ Tissue repairing	Ref
Fibrin glue	＞3min	~5 kPa	Direct adhesion	N/R	N/R	FDA-Approved product
Cyanoacrylate glue	Instant	~20 kPa	Direct adhesion	N/R	N/R	FDA-Approved product
O-nitrobenzene modified carboxymethyl chitosan	Dozens of seconds	77.8 kPa （pig saline）	UV irrdation	Yes	Yes	[18]
Chitooligosaccharide / poly(N-acryloyl 2-glycine)	Instant	208 J m^{-2} (pig skin)	Direct adhesion	N/R	Yes	[19]
HEMA/NVP/ PAA-NHS	Instant	300 J m^{-2} ~50 kPa (pig gastric)	Direct adhesion	N/R	N/R	[20]

Materials & Forms	Adhesion speed	Wet adhesion properties	Adhesion condition	Antibacterial properties	Wound Healing/ Tissue repairing	Ref
Poly(acrylamide-methyl acrylate-acrylic acid)	180 s	124 J m^{-2} ~12 kPa (pig small intestine)	UV irritation	N/R	N/R	[21]
PAM /PDA/ silica nanoparticles	Instant	151 J m^{-2} ~17 kPa (pig skin)	Direct adhesion	N/R	N/R	[22]
PAA-NHS/ 4VPBA/ isocyanatoethyl / polyols	＜5 s	400 J m^{-2} (pig skin)	Direct adhesion	N/R	N/R	[23]
PAM /PSBMA /Laponite XLG/TA	Instant	59.7 J m^{-2} (pig skin)	Direct adhesion	N/R	N/R	[24]
PVA/PAA-S-S-NHS	＜5 s	~400 J m^{-2} (pig skin)	Direct adhesion	N/R	N/R	[25]
ε-PL-Cat/ oxidized dextran	30 min	~15 kPa (pig skin)	Direct adhesion	N/R	YES	[26]
PAM/ chitosan/ PU/PAA	Instant	853 J m^{-2} (pig skin)	Direct adhesion	N/R	N/R	[27]

Materials & Forms	Adhesion speed	Wet adhesion properties	Adhesion condition	Antibacterial properties	Wound Healing/ Tissue repairing	Ref
Tyr/phenylalanine	2 h	26.66 kPa (pig skin)	Direct adhesion	N/R	YES	[28]
Alg-DA/ PAA	＜10 s	~78 kPa （pig vessels)	Direct adhesion	N/R	N/R	[29]
Chitosan/PNIPAM/ PET	60 min	120 J m^{-2} (pig skin)	EDC/NHS Surface treatment	N/R	N/R	[30]
Gallic acid/ chitosan/ γ-PGA/PEGS-NH2	30 s	~400 J m^{-2} 46.1 kPa (pig skin)	Injection	N/R	N/R	[31]
Protocatechualdehyde QCS/ Fe3+	3 h	~40 kPa (pig skin)	Injection	YES	YES	[32]
TA/CS/ fibroin/Alg/ Ag NPs	40 min	151 kPa (pig skin)	Direct adhesion	YES	YES	[33]
Alg / 3APBA	10 min	2.0 ± 7.2 kPa	10X PBS curing	N/R	N/R	[34]

Materials & Forms	Adhesion speed	Wet adhesion properties	Adhesion condition	Antibacterial properties	Wound Healing/ Tissue repairing	Ref
GO/PVA/PAA-NHS	＜5 s	~270 J m^{-2} ~60 kPa. (pig skin)	Direct adhesion	N/R	N/R	[35]
Epigallocatechin-3-gallate /3-AMPBA	5 min	7.06 kPa (pig skin)	Direct adhesion	YES	YES	[36]
Glycerin/PVA/PAA-NHS/borax	**＜3 min**	**~600 J m^{-2} 70 kPa (pig skin)**	**Direct adhesion**	**YES**	**YES**	**Our work**

Table S5. Comparison of hydrogels-based bioelectronics in different categories.

Materials (hydrogel)	Mechanical property (Modulus)	Conductivity (S cm^{-1})	Adhesion properties	Bio-compatibility (in vivo cytotoxicity)	Transparency	Application	Ref
PDA-reduced sulfonate GO /PEDOT	E=11 GPa	8.296	~20 kPa (pig skin)	Non-toxic	NO	Bioelectrode for detecting ECG, EEG, and EMG signals.	[37]
PEDOT: PSS/PVA	E≈460 kPa	10	~600 J m^{-2}	Non-toxic	NO	EMG electrodes	[38]
Fibroin/ rGO/TA	E=20 MPa	~1x10^{-2}	~20 kPa (pig skin)	Non-toxic	NO	Bionic glove	[39]
GO/PVA/ PAA-NHS	E=293 kPa	~2.6 x 10^{-2}	~270 J m^{-2} ~60 kPa (pig skin)	Non-toxic	NO	Electrical bio-adhesive interface for bio-electronics	[35]
Pyrrole/ gelatin/ dopamine/ Fe^{3+}	G‘=34.7 kPa	6.51 x 10^{-4}	60 J m^{-2} 22.2 kPa (Pig myocardium tissue)	Non-toxic	NO	Therapeutic Cardiac Patches	[40]
Poly(SBVD/ graphite	G‘=8.04 kPa	3.75 x 10^{-5}	54 kPa (pig skin)	Non-toxic	NO	Neuromodulation interface electrode	[41]
Glycerin/ PVA/PAA-NHS/borax	**G’=12 kPa**	**3.62 x 10^{-2}**	**~600 J m^{-2} ~70 kPa (pig skin)**	**Non-toxic**	**YES**	**Neuromodulation**	**Our work**

References

1. L. Leibler, E. Pezron and P. A. Pincus, *Polymer*, 1988, **29**, 1105-1109.

2. X. Pan, Q. Wang, P. He, K. Liu, Y. Ni, L. Chen, X. Ouyang, L. Huang, H. Wang and S. Xu, *Chem. Eng. J.*, 2020, **379**, 122271.

3. W.-P. Chen, D.-Z. Hao, W.-J. Hao, X.-L. Guo and L. Jiang, *Acs Appl Mater Inter*, 2018, **10**, 1258-1265.

4. X. P. Morelle, W. R. Illeperuma, K. Tian, R. B. Bai, Z. G. Suo and J. J. Vlassak, *Adv. Mater.*, 2018, **30**, 1801541.

5. C. M. Tringides, N. Vachicouras, I. de Lazaro, H. Wang, A. Trouillet, B. R. Seo, A. Elosegui-Artola, F. Fallegger, Y. Shin, C. Casiraghi, K. Kostarelos, S. P. Lacour and D. J. Mooney, *Nature Nanotechnology.*, 2021, **16**, 1019.

6. C. Mmab, D. Am, E. Bd, D. Nf, D. Jvs and B. Mg, *Brain Multiphysics.*, 2020, **1**, 100018.

7. E. Giannessi, M. R. Stornelli, A. Coli and P. N. Sergi, *Applied Sciences-Basel.*, 2019, **9**, 1115.

8. Harter, JM, Varghese, Kliewer, MA, DeWall, RJ, Hartenbach and EM, *Ultrasonic Imaging.*, 2010, **32**, 214.

9. G. Constantinides, Z. I. Kalcioglu, M. McFarland, J. F. Smith and K. J. Van Vliet, *Journal of Biomechanics.*, 2008, **41**, 3285.

10. E. J. Chen, J. Novakofski, W. K. Jenkins and W. D. O. Brien, *IEEE Transactions on Ultrasonics, Ferroelectrics, and Frequency Control.*, 1996, **43**, 191.

11. S. L. Barnes, A. Lyshchik, M. K. Washington, J. C. Gore and M. I. Miga, *Medical Physics.*, 2007, **34**, 4439.

12. B. K. Tay, J. Kim and M. A. Srinivasan, *Ieee Transactions on Biomedical Engineering.*, 2006, **53**, 2129.

13. D. M. Ebenstein and L. A. Pruitt, *J. Biomed. Mater. Res.*, 2004, **69A**, 222.

14. J. G. Jacot, S. Dianis, J. Schnall and J. Y. Wong, *J. Biomed. Mater. Res.*, 2006, **79A**, 485.

15. A. Lundkvist, E. Lilleodden, W. Siekhaus, J. Kinney, L. Pruitt and M. Balooch, *MRS Online Proceedings Library.*, 1996, **436**, 353.

16. T. Oie, Y. Murayama, T. Fukuda, C. Nagai, S. Omata, K. Kanda, H. Yaku and Y. Nakayama, *J Artif Organs.*, 2009, **12**, 40.

17. A. J. Engler, L. Richert, J. Y. Wong, C. Picart and D. E. Discher, *Surf. Sci.*, 2004, **570**, 142.

18. Y. F. Ma, J. X. Yao, Q. Liu, T. Han, J. P. Zhao, X. H. Ma, Y. M. Tong, G. R. Jin, K. Qu, B. Q. Li and F. Xu, *Adv. Funct. Mater.*, 2020, **30**, 2001820.

19. C. Y. Cui, T. L. Wu, X. Y. Chen, Y. Liu, Y. Li, Z. Y. Xu, C. C. Fan and W. G. Liu, *Adv. Funct. Mater.*, 2020, **30**, 2005689.

20. X. M. Chen, J. Zhang, G. D. Chen, Y. Xue, J. J. Zhang, X. Y. Liang, E. M. Lei, J. S. Lin, B. B. Xu and J. Liu, *Adv. Funct. Mater.*, 2022, **32**, 2202285.

21. A. H. C. Anthis, X. Q. Hu, M. T. Matter, A. L. Neuer, K. C. Wei, A. A. Schlegel, F. H. L. Starsich and I. K. Herrmann, *Adv. Funct. Mater.*, 2021, **31**, 2007099.

22. H. Jung, M. K. Kim, J. Y. Lee, S. W. Choi and J. Kim, *Adv. Funct. Mater.*, 2020, **30**, 2004407

23. Y. Xue, J. Zhang, X. M. Chen, J. J. Zhang, G. D. Chen, K. Zhang, J. S. Lin, C. A. F. Guo and J. Liu, *Adv. Funct. Mater.*, 2021, **31**, 2106446.

24. G. G. Yang, K. H. Zhu, W. Guo, D. R. Wu, X. L. Quan, X. Huang, S. Y. Liu, Y. Y. Li, H. Fang, Y. Q. Qiu, Q. Y. Zheng, M. L. Zhu, J. Huang, Z. G. Zeng, Z. P. Yin and H. Wu, *Adv. Funct. Mater.*, 2022, **32**, 2200457.

25. X. Y. Chen, H. Yuk, J. J. Wu, C. S. Nabzdyk and X. H. Zhao, *Proceedings of the National Academy of Sciences of the United States of America.*, 2020, **117**, 15497.

26. S. Li, N. Chen, X. Li, Y. Li, Z. Xie, Z. Ma, J. Zhao, X. Hou and X. Yuan, *Adv. Funct. Mater.*, 2020, **30**, 2000130.

27. C. H. Wang, X. Y. Chen, L. Wang, M. Makihata, H. C. Liu, T. Zhou and X. H. Zhao, *Science*, 2022, **377**, 517.

28. J. Deng, Y. Y. Tang, Q. Zhang, C. Wang, M. Liao, P. Ji, J. L. Song, G. X. Luo, L. Chen, X. H. Ran, Z. M. Wei, L. W. Zheng, R. Y. Dang, X. Liu, H. M. Zhang, Y. S. Zhang, X. M. Zhang and H. Tan, *Adv. Funct. Mater.*, 2019, **29**, 1809110.

29. B. Xue, J. Gu, L. Li, W. Yu, S. Yin, M. Qin, Q. Jiang, W. Wang and Y. Cao, *Nat Commun*, 2021, **12**, 7156.

30. Y. Gao, X. Han, J. Chen, Y. Pan, M. Yang, L. Lu, J. Yang, Z. Suo and T. Lu, *Proceedings of the National Academy of Sciences*, 2021, **118**, e2103457118.

31. K. Chen, Z. H. Wu, Y. T. Liu, Y. Yuan and C. S. Liu, *Adv. Funct. Mater.*, 2022, **32**, 2109687.

32. Y. Liang, Z. Li, Y. Huang, R. Yu and B. Guo, *ACS Nano*, 2021, **15**, 7078.

33. G. X. Pan, F. H. Li, S. H. He, W. D. Li, Q. M. Wu, J. J. He, R. J. Ruan, Z. X. Xiao, J. Zhang and H. H. Yang, *Adv. Funct. Mater.*, 2022, **32**, 2200908.

34. S. H. Hong, M. Shin, E. Park, J. H. Ryu, J. A. Burdick and H. Lee, *Adv. Funct. Mater.*, 2020, **30**, 1908497

35. J. Deng, H. Yuk, J. J. Wu, C. E. Varela, X. Y. Chen, E. T. Roche, C. F. Guo and X. H. Zhao, *Nature Materials.*, 2021, **20**, 229.

36. X. D. Zhao, D. N. Pei, Y. X. Yang, K. Xu, J. Yu, Y. C. Zhang, Q. Zhang, G. He, Y. F. Zhang, A. Li, Y. L. Cheng and X. S. Chen, *Adv. Funct. Mater.*, 2021, **31**, 2009442.

37. D. L. Gan, Z. Q. Huang, X. Wang, L. L. Jiang, C. M. Wang, M. Y. Zhu, F. Z. Ren, L. M. Fang, K. F. Wang, C. M. Xie and X. Lu, *Adv. Funct. Mater.*, 2020, **30**, 1907678.

38. G. Li, K. X. Huang, J. Deng, M. X. Guo, M. K. Cai, Y. Zhang and C. F. Guo, *Adv. Mater.*, 2022, **34**, 2200261.

39. F. B. Kadumudi, M. Hasany, M. K. Pierchala, M. Jahanshahi, N. Taebnia, M. Mehrali, C. F. Mitu, M. A. Shahbazi, T. G. Zsurzsan, A. Knott, T. L. Andresen and A. Dolatshahi-Pirouz, *Adv. Mater.*, 2021, **33**, 2100047

40. S. Liang, Y. Y. Zhang, H. B. Wang, Z. Y. Xu, J. R. Chen, R. Bao, B. Y. Tan, Y. L. Cui, G. W. Fan, W. X. Wang, W. Wang and W. G. Liu, *Adv. Mater.*, 2018, **30**, 1704235.

41. I. K. Han, K. I. Song, S. M. Jung, Y. Jo, J. Kwon, T. Chung, S. Yoo, J. Jang, Y. T. Kim, D. S. Hwang and Y. S. Kim, *Adv. Mater.*, 2023, **35**, 2203431